REPORT DOCUMENTATION PAGE

Form Approved
OMB No. 0704-0188

1. REPORT DATE *(DD-MM-YYYY)*	2. REPORT TYPE	3. DATES COVERED *(From - To)*
26-04-2007	Final Report	3/15/04 - 12/31/06

4. TITLE AND SUBTITLE
High Performance Polymer Memory and Its Formation

5a. CONTRACT NUMBER

5b. GRANT NUMBER
FA9550-04-1-0215

5c. PROGRAM ELEMENT NUMBER

6. AUTHOR(S)
Prof. Yang Yang

5d. PROJECT NUMBER

5e. TASK NUMBER

5f. WORK UNIT NUMBER

7. PERFORMING ORGANIZATION NAME(S) AND ADDRESS(ES) AND ADDRESS(ES)
Department of Materials Science and Engineering
UCLA
6531 Boelter Hall
Los Angeles, CA 90095
Tel: 310-825-4052
Fax: 310-206-7353

8. PERFORMING ORGANIZATION REPORT NUMBER

9. SPONSORING / MONITORING AGENCY NAME(S) AND ADDRESS(ES)
USAF, AF Office of Scientific Research
875 North Randolph St.,
Suite 325, Room 3112
Arlington, VA 22203
Dr Charles Lee/NA

10. SPONSOR/MONITOR'S ACRONYM(S)

11. SPONSOR/MONITOR'S REPORT NUMBER(S)

12. DISTRIBUTION / AVAILABILITY STATEMENT
Distribute to the public.

AFRL-SR-AR-TR-07-0176

13. SUPPLEMENTARY NOTES

14. ABSTRACT

Under the major support from AFOSR (**FA9550-04-1-0215)** during the years of 2004, 2005 and 2006, we have done significant achievement on scientific research and invented very promising electronic and optoelectronic devices including (1) nano-composite polymer memory devices based on metal-nanoparticles and nano-structured virus biomaterials, (2) vertical organic transistors, (3) efficient polymer solar cells, and (4) high efficient polymer light emitting diodes. We totally published 32 papers in the first rated referee journals and filed 8 patents. Some of the developed technologies have been transferred to industry for commercialization (see the attached table).

15. SUBJECT TERMS

16. SECURITY CLASSIFICATION OF:			17. LIMITATION OF ABSTRACT	18. NUMBER OF PAGES	19a. NAME OF RESPONSIBLE PERSON
a. REPORT	b. ABSTRACT	c. THIS PAGE		25	19b. TELEPHONE NUMBER *(include area code)*

Final Report to AFOSR

High Performance Polymer Memory Device and Its Formation

Fund No.: FA9550-04-1-0215

Prepared by Prof. Yang Yang
Department of Materials Science and Engineering
University of California-Los Angeles
Los Angeles, CA 90095

Date: April 26, 2007

Abstract

Under the major support from AFOSR (**FA9550-04-1-0215**) during the years of 2004, 2005 and 2006, we have done significant achievement on scientific research and invented very promising electronic and optoelectronic devices including (1) nano-composite polymer memory devices based on metal-nanoparticles and nano-structured virus biomaterials, (2) vertical organic transistors, (3) efficient polymer solar cells, and (4) high efficient polymer light emitting diodes. We totally published 32 papers in the first rated referee journals and filed 8 patents. Some of the developed technologies have been transferred to industry for commercialization (see the following table).

Company Name	**Location**	**Technology**	**Year**
Coatue Technology (start-up)	Boston	Organic Memory	2001 – 2003 (acquired by AMD)
ORFID Corp (start-up)	Los Angeles	Vertical Organic Transistor	2004 – now
Rohm Haas	Philadelphia	Polymer Memory	2004 and 2005
Adesto (start-up)	San Jose	Organic Memory	2006 (in negotiation)
Solarmer	Los Angeles	Polymer solar cell	2006-now
Silanna	Australia	Memory	2006 (in negotiation)

Part 1. Polymer memory based on Au-nanoparticles

We developed a polymer bistable device by a very simple solution processing approach. The electrical bistable nature of the device indicates that it has a very strong application potential as an ultrahigh density and ultra-fast electronic memory. We studied the device performance by using different materials for the device. We studied the temperature dependence of the device characteristics and presented a model to explain the mechanism of electrical switching in the device. By exploiting an electric-field induced charge transfer between the metal nanoparticles and small conjugated organic compounds, the device exhibited electric-field programmable two conductivity states. It has remarkable advantages: the materials used in this device are readily available and easily controlled, the device can be fabricated through a simple solution processing approach, the response time is very short, and the operating voltages are low. The device has a high flexibility so that it is compatible with other organic devices. In addition, the device with multiple active layers could be readily constructed so that the density could be further increased. This last advantage is significant compared to traditional inorganic semiconductor memory, which is restricted to two dimensions.

1.1 Electrical tests and its application as nonvolatile memory

The polymer memory device has a simple device structure with a polymer film sandwiched between two metal electrodes (Fig. 1). The polymer film consists of Au nanoparticles capped with 1-dodecanethiol (Au-DT NP), 8-hydroxyquinoline (8HQ) and polystyrene (PS). The metal nanoparticles were prepared by the two-phase

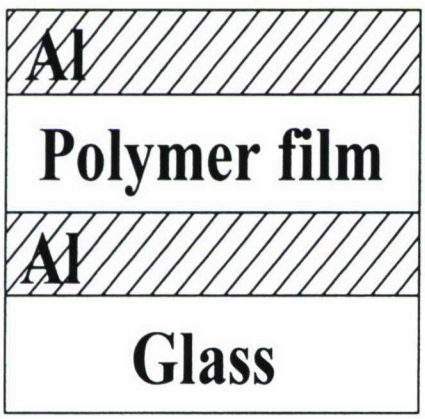

Fig. 1 Device structure.

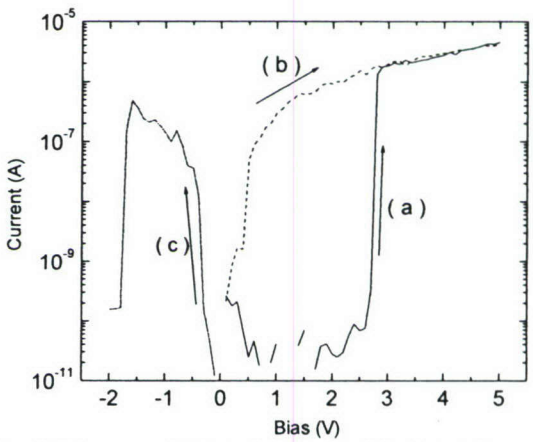

Fig. 2 IV curve of Al/Au-DT+8HQ+PS/Al. (a) first scan, (b) second scan, and (c) third scan.

arrested growth method and had a narrow size distribution (1.6 - 4.4 nm in diameter) and an average particle size of 2.8 nm. The device was fabricated through a very simple process. Glass was used as the substrate, and the top and bottom Al electrodes were formed by thermal evaporation in high vacuum. The active layer was fabricated

by spin-coating a 1,2-dichlorobenzenic solution of 0.4% Au-DT NP by weight, 0.4% 8HQ by weight, and 1.2% PS by weight. This device is represented by Al/Au-DT+8HQ+PS/Al.

The current-voltage (I-V) curves of this device are shown in Fig. 2. The device exhibited very low current, approximately 10^{-11} A, at 1 V in vacuum. An electrical transition took place at 2.8 volts with an abrupt current increase from 10^{-11} A to 10^{-6} A (curve (a)). The device exhibited good stability in this high conductivity state during the subsequent voltage scan (curve (b)). The high conductivity state was able to return to the low conductivity state by applying a negative bias, as indicated in curve (c), where the current suddenly dropped to 10^{-10} A at -1.8 V. Whether tested under a nitrogen atmosphere or in air, the device exhibited similar electrical behavior. The presence of oxygen and moisture in the environment did not affect the threshold voltages for the electrical transitions and the currents in the high conductivity state, but it caused the current in the low conductivity state to be one order of magnitude higher than that in vacuum.

Switching between the high and low conductivity states of Al/Au-DT +8HQ+PS/Al was performed numerous times. The device was written, read, and erased in air repeatedly, as demonstrated in Fig. 3, (for convenience the absolute value of the current is shown). A voltage of 5 V was applied to write "1" to the device, that is, this voltage switched the device to the high conductivity state. (Here we designate "1" as the high conductivity state, and "0" as the low conductivity state.) This "1" state could be read by a low voltage (1.1 V in our case). The current during the read pulse was in the range of 10^{-7} A. This high conductivity state was erased by a voltage of -2.3 V which returned the device to the low conductivity "0" state. This "0" state could also be detected by applying a small voltage. The current here was in the range of 10^{-9} A. These write-read-erase cycles demonstrate that the device can be used as a nonvolatile memory device.

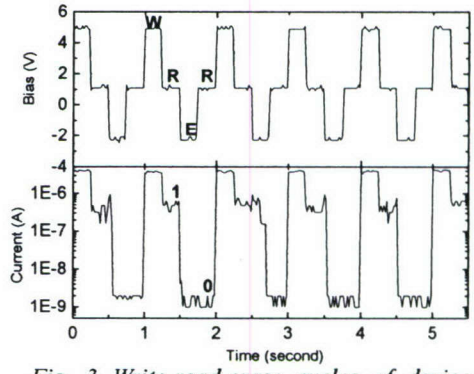

Fig. 3 Write-read-erase cycles of device Al/Au-DT+8HQ+PS/Al. The top and bottom curves are the applied voltage and the corresponding current response, respectively.

The device in the low conductivity state could be turned to the high conductivity state by applying a pulse of 5 volt with a width of 25 nanoseconds, with instrument limitations on the width of the pulse. So, the actual response time could even be shorter than 25 nanoseconds.

The device in the low conductivity state always exhibits very low current at a

voltage of 1 V, while the stability in the high conductivity state is device dependent. We got a device which exhibits stability in the high conductivity state longer than 50 hours.

These experimental results demonstrate that this device can be used as a high-density, ultra-fast, and nonvolatile memory device. Combining these characteristics with the light weight and high flexibility, this device will be very useful for satellite applications.

1.2. Study of the Effect of Materials on Device Performance

Devices were fabricated using different materials. The performance of this device is strongly dependent on the materials used. When 8HQ was replaced by 9,10-dimethylanthracene (DMA), the device exhibited an electrical transition at 6.1 volts from the low to the high conductivity state, while the threshold voltage from the high to low conductivity state appeared at about -2.9 V.

When an additional layer was added, the device performance changed as well. The switching behaviors were symmetrical in the two biased directions, that is, the transition voltage from the low to the high conductivity took place at almost the same

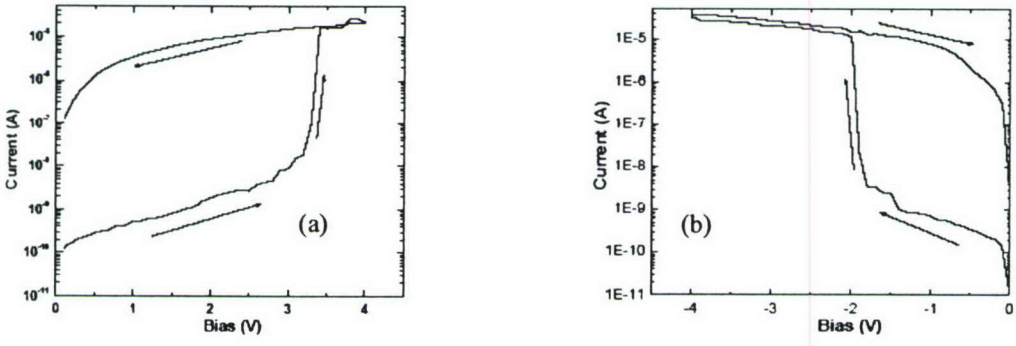

Fig. 4 (a) IV curves when the top electrode was positively biased. (b) IV curves when the top electrode was negatively biased. The arrows in the (a) and (b) denote the bias-scanning directions.

absolute voltage value regardless that the top electrode was positively or negatively biased. However, asymmetrical switching behaviors were observed when an additional N,N'-Bis(naphthalene-1-yl)-N,N'-bis(phenyl)benzidine (NPB) layer was thermally deposited on the film consisting of Au-DT NP, 8HQ and PS. This device was denoted by Al (top)/NPB/Au-DT+8HQ+PS/Al (bottom)/glass. The transition from the low to high conductivity state appeared at about 3.3 V when the top electrode was positively biased (Fig. 4a), while it changed to about -1.9 V when the device was reversely biased (Fig. 4b).
the (a) and (b) denote the bias-scanning directions.

The chemical structure of the capping molecule on the Au nanoparticles has a strong effect on the IV curve as well. When the capping molecule was a conjugated 2-naphthalenethiol (2NT), the device exhibited current increase not abruptly, and the device in the high conductivity state could not be returned to the low conductivity state by applying a negative or a positive voltage (Fig. 5).

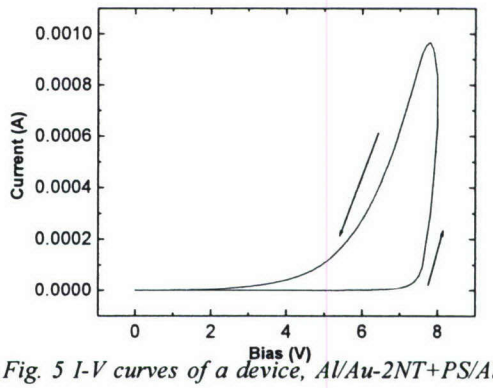

Fig. 5 I-V curves of a device, Al/Au-2NT+PS/Al. The arrows indicate the voltage-scanning directions.

1.3. Study of the Mechanism for Electrical Switching

The conduction mechanism for Al/Au-DT+8HQ+PS/Al in the low conductivity state may be due to quite small amount of impurity or hot electron injection. For the device in the high conductivity state, the I-V curves were measured from room temperature down to liquid nitrogen temperature to study the conduction mechanism. Fig. 6 is the Arrhenius plot of the temperature dependence of the current. The activation energy was 1-1.7 meV for an applied voltage of 1 to 4 V. This activation energy was so small that the current was almost independent of the temperature.

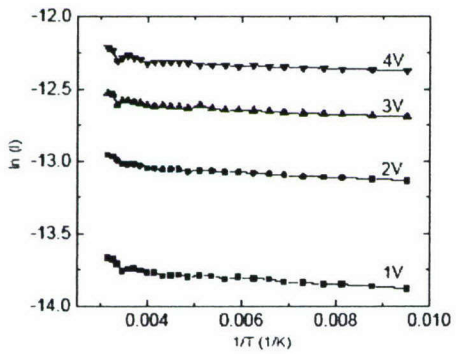

Fig. 6 Arrhenius plot of temperature dependence of current for Al/Au-DT+8HQ+PS/Al in the high conductivity state, at applied voltages of 1, 2, 3, and 4 V.

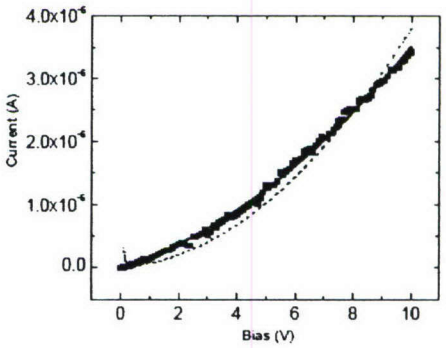

Fig. 7 I-V curve of the device, Al/Au-DT+8HQ+PS/Al, in the high conductivity state. The scattered points are the experimental results, the solid line is the data fit combining Direct tunneling and Fowler-Nordheim tunneling, and the broken line is the data fit of Fowler-Nordheim

These experimental results suggested that the electrical current in the high conductivity state would be due to some temperature-independent charge tunneling processes. The IV curves could be fitted well by a combination of Direct tunneling (tunneling through a square barrier) and Fowler-Nordheim tunneling (tunneling through a triangular barrier) as given by the following expression (Fig. 7)

$$I = C_1 V e^{-\frac{2d\sqrt{2m^*\Phi}}{\hbar}} + C_2 V^2 e^{-\frac{4d\Phi^{3/2}\sqrt{2m^*}}{3q\hbar V}}$$

The first term on the right hand side of the equation is the current contributed by direct tunneling, and the second term is the current contributed by Fowler-Nordheim tunneling. In this equation, d is the tunneling distance, m^* is the effective mass of the charge carrier, and Φ is the energy barrier height. At low voltage, V<Φ, direct tunneling is the dominant conduction mechanism, and at high voltage, V>Φ, Fowler-Nordheim tunneling becomes the dominant conduction mechanism.

The different conduction mechanisms in the two states suggested change in the electronic structure of the device after the electrical transition. We proposed a charge transfer between Au-DT NP and 8HQ under a high electric field. Prior to the electronic transition there is no interaction between the Au-DT nanoparticles and 8HQ. Concentration of charge carriers due to impurity in the film is quite low, so that the film has very low conductivity. However, when the electrical field increases to a certain value, electron on the HOMO of 8HQ may gain enough energy to tunnel through the capped molecule, dodecanethiol, into Au nanoparticles. Consequently, the HOMO of 8HQ becomes partially filled, and 8HQ and Au nanoparticles are charged positively and negatively, respectively. Therefore, carriers are generated and the device exhibits a high conductivity state after the charge transfer.

For the device in the high conductivity state, it was proposed that charge transport through the polymer film may take place through charge tunneling among the 8HQ molecules. The separation among the 8HQ molecules in the polymer film will be larger than that in the 8HQ crystal. A simple estimation of the separation among the 8HQ molecules in the Au-DT+8HQ+PS film suggested that it is reasonable for the tunneling process to become the dominant charge transport mechanism among the 8HQ molecules. The barrier between two neighboring 8HQ may change from a square barrier to a triangular barrier with the increase of the applied voltage, which leads to the change of the IV curve from direct tunneling to Fowler-Nordheim tunneling.

This simple model could interpret the stability of the device in the high conductivity state and the erasing process by applying a negative bias as well. Stability of the negative charge on Au nanoparticles is due to the insulator coating, dodecanethiol, on the Au nanoparticles, which prevents recombination of the charge after removal of the external electric field. Since the charge transfer is induced by an external electrical field, the film is polarized after the charge transfer. Only a reverse electric field can assist the tunneling of the electron from the Au nanoparticles into the HOMO of $8HQ^+$, resulting in a return to the low conductivity state.

Part 2. Virus-nanoparticles Hybrid Memory Device

A hybrid memory device based on Tobacco Mosaic Virus (TMV) and platinum nanoparticles was successfully demonstrated. **This is the first time electronic functionality is introduced to a virus conjugated with nanoparticles.** Using electroless deposition in a platinum ion solution, the nanoparticles were attached to specific functional groups on the protein surface of the virus. As a result, a very uniform distribution of the nanoparticles on the virus surface was obtained (Figure 8a). The memory device was then fabricated by sandwiching the bio-inorganic hybrid nanocomposite embedded in a polyvinyl alcohol matrix between two aluminum electrodes.

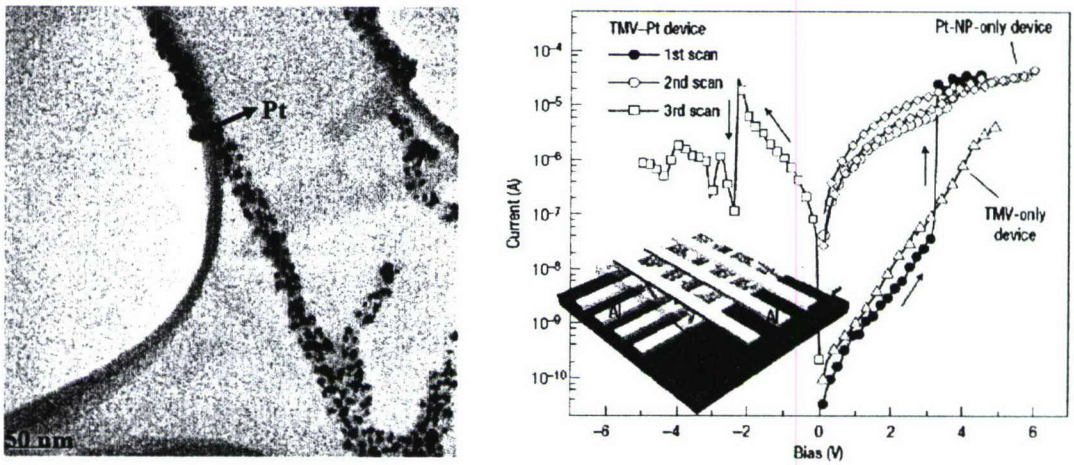

Figure 8: a) TEM image of the TMV-Pt conjugate, b) I-V characteristics of TMV-Pt hybrid memory device (inset: crossbar structure of memory device)

Figure 8b shows the crossbar array structure and the I-V characteristics of the memory device. When sweeping the voltage applied to the device, the conductivity switched from a low to a high conductivity state at a threshold voltage of about 3V. The device remained in the high conductivity state even when the voltage was returned to 0V. The conductivity state was reverted back to its original low state at a reverse bias of about -2.4V. The switching between the two conductivity states could also be performed using short electrical pulses. Since, the two conductivity states are stable even when no external voltage is applied to it, this device can function as a nonvolatile memory storage device

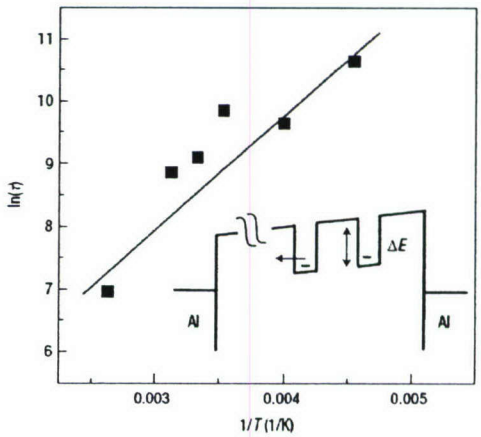

Figure 9: Arrhenius plot of the charge retention time versus inverse temperature

with the two states representing "1" and "0" of the information bit.

The switching mechanism of the device is due to the electric field induced charge transfer between the virus and the nanoparticles. In the high conductivity state, the charge is stored in the platinum nanoparticles and stabilized by the coat protein of the virus. A negative electric field is needed to overcome the barrier to reverse the charge transfer. A temperature dependence study of the retention time of the device was performed to estimate the barrier height of the charge trap. The activation energy was approximated to be about 0.15eV from the Arrhenius plot of the charge retention time (Figure 9).

This work was published in the first issue of Nature Nanotechnology. The new concept of conjugating biomolecules with nanoparticles opens up new possibility for incorporating

Part 3. Accurate Measurement and Characterization of Organic Solar Cells

(1). Introduction

Organic solar cells have attracted much attention in the last several years and today are considered a promising source for clean and renewable energy.[1-6] Organic solar cells are divided into two main categories: ones based on conjugated polymers are the so-called bulk-heterojunction (BHJ) solar cells,[7,8] and the others based on small organic molecules are bilayer heterojunction structures.[9] In polymer-based BHJ solar cells, the most common donor polymers that have been used in the past are poly[2-methoxy-5-(3,7-dimethyloctyloxy)-1,4-phenylene vinylene] (MDMO-PPV),[10-12] regioregular poly(3-hexylthiophene) (RR-P3HT),[13-20] and poly[2-methoxy-5-(2'-ethyl-hexyoxy)-1,4-phenylene vinylene] (MEH-PPV)[7,21-22]. The most common candidate for the acceptor material is [6,6]-phenyl C_{61}-butyric acid methyl ester (PCBM).[23] On the other hand, several small molecules such as copper pthalocyanine (CuPc),[24-26] zinc pthalocyanine (ZnPc),[27,28] tetracene,[29] and pentacene[30] have been used as donors combined with buckminsterfullerene (C_{60}) molecules in a bilayer heterojunction.

The highest power conversion efficiency (PCE) reported so far for polymer BHJ solar cells is up to 5%, for devices based on P3HT.[18-20] For small molecule-based solar cells, efficiencies up to 6.0% have been reported for devices based on CuPc.[25] As a result of continuing research efforts, the efficiencies of organic solar cells are now fast approaching the levels where they could be put into commercial applications. For the healthy development of this technology, it is now critical to accurately determine the efficiency values for a fair comparison with results from different research groups. Significant efforts have been made in the past to accurately determine the efficiency of solar cells, and a standard test method has been established.[31-33] In 1980 the Cell Performance Laboratory was established by DOE at NREL to provide the U.S. terrestrial PV community with standardized efficiency measurement and reference cell calibrations. In the early 1980's similar laboratories were being set up in Germany, Japan and elsewhere. In the 1980's U.S. and international standards were developed and adopted by the national PV calibration laboratories around the world.[30,31]

Unfortunately, for organic solar cells, these internationally accepted norms are seldom followed at the research level, partially due to lack of awareness of these norms, limited resources, and/or relatively low efficiency. As a result, efficiency values under various testing conditions have been reported, which makes reliable comparison between data from different research groups very difficult. Some efforts in the past have sought to motivate the organic solar cell community toward adopting standards for accurately measuring efficiency.[34-35] In this paper, the research group at the University of California, Los Angeles (UCLA), has collaborated with the National Renewable Energy Laboratory (NREL), Colorado, to present a simple method to

accurately determine the efficiency of organic solar cells. Different kinds of test cell / reference cell combinations have been used to calculate the spectral mismatch factors under the standard reference spectrum. We also demonstrate the importance of choosing a suitable reference cell for light-source intensity calibration.

(2) Light Source Calibration and Spectral Mismatch Factor An important factor in the solar simulator calibration procedure is the relative spectral responsivities of the test and reference cells. Typically, for crystalline solar cells, the reference cell is made of the same materials and technology as the test device, which results in M being closer to unity. Of primary importance in a reference cell is the stability in the reference cells calibration value. For this reason most thin-film organic and inorganic devices use a Si reference cell that may have a filter to improve the spectral match. However, for polymer and organic solar cells, it is extremely difficult to fabricate reference cells from the same materials. The reasons for this are the relatively underdeveloped fabrication techniques that lack consistent reproducibility, and poor lifetimes of these devices. Therefore, for the purpose of light-source calibration for organic solar cell testing, it is important to select a reference cell whose spectral response matches that of the actual test cells as closely as possible to minimize the spectral error which is not being numerically corrected for. The spectral responsivities of the two reference cells we selected are shown in Figure 10(a). The unfiltered Si diode shows significant response in the wavelength range of 400-1100 nm. However, the response for Si diode with KG5 color filter is exhibited in a wavelength range of 350-700 nm. Clearly, the responsivity of the latter is similar to the responsivity of our test cells, making it more suitable for use in calibrating the light intensity of the solar simulator. This argument is further supported by calculating the mismatch factor for the four different test cells, using both the reference cells. For the purpose of calculating M under AM 1.5 G standard conditions, the reference spectrum used is the AM 1.5 G standard spectrum (IEC 60904),[37] and the source irradiance spectrum is the

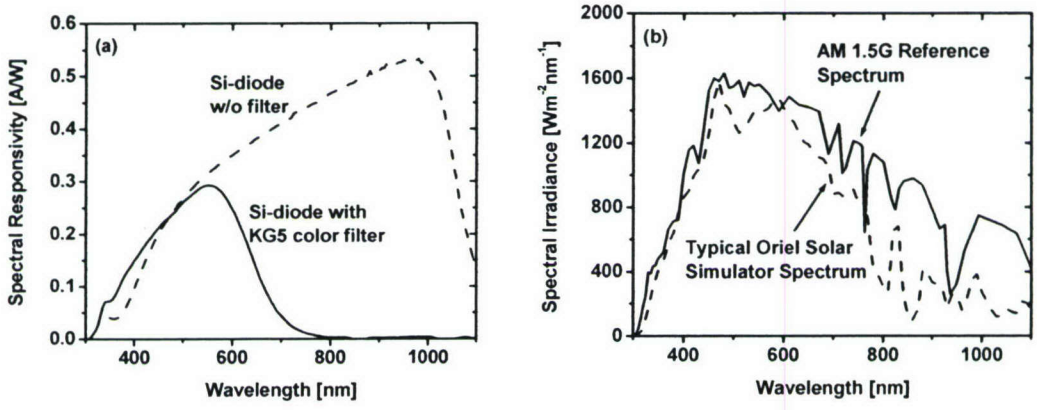

Figure 1 (a) Spectral responsivities of two types of reference cells: an unfiltered monocrystalline Si diode and a Si diode with KG5 color filter. (b) Spectral irradiance data for AM 1.5 G reference spectrum (IEC 60904) (Ref. 35) and the typical source irradiance for Oriel 150 W solar simulator with AM 1.5 G filters (obtained

typical irradiance spectrum for the Oriel 150 W solar simulator with AM 1.5 G filter (obtained from Newport Corporation). The reference and the source spectra used for calculating *M* are shown in Figure 1(b). It should be noted that the spectra of the light sources depend on a number of factors, and the actual irradiance of the light source may be different from the typical spectrum that is shown here. The factors that can affect the irradiance spectrum of the light source are the age of the lamp, optical setting of that particular lamp, and current through the lamp. However, the aim here is to obtain "typical" spectral mismatch factor values for different test cell / reference cell combinations using a generic source spectral irradiance. The *M* values calculated by using the spectral responsivity data for different test cell / reference cell combinations are summarized in Table I. Using a Si diode with KG5 color filter as a reference cell for light-source calibration clearly has an advantage over an unfiltered Si diode. The mismatch-factor values are very close to unity for all test cell / KG5 filtered Si-diode combinations, whereas the mismatch is between 31% and 35 % for all test cell / unfiltered Si-diode combinations. This suggests that when an unfiltered Si diode is used for calibrating the light-source intensity, possible errors due to spectral mismatch can be as high as 35%. Once M is known for a specific test cell / reference cell combination under the source spectrum, the short-circuit current of the test device under the reference spectrum can be calculated. A mismatch factor can therefore be used to correct the efficiency values with minimal error. Mismatch factors have been used in the past to correct the efficiency values for polymer BHJ solar cells.[11] We mentioned earlier that the actual irradiance of a light source depends on several factors, one of which is the age of the lamp. As a result the spectral mismatch would change with the solar simulator's lamp age. Figure 2 shows the spectral mismatch factor for a P3HT:PCBM(DCB) test cell as a function of lamp age. The light source is a Spectrolab X25 solar simulator operating at one sun. We used two different reference cells (unfiltered and KG5-filtered Si diodes) for calculating *M*. For the unfiltered Si reference cell the mismatch varied by more than 10% over 900 hours. However, for the KG-filtered mono-Si cell the mismatch varied by only 1% over 900 hours.

Test Cell Type	Mismatch Factor	
	Si diode with KG5 color filter	Unfiltered Si diode
MEHPPV:PCBM	0.99	1.32
P3HT:PCBM(DCB)	1.01	1.35
P3HT:PCBM(CB)	1.01	1.35

Table I. Spectral mismatch factors calculated with respect to the AM 1.5 G reference spectrum (IEC 60904) (Ref. 35) for various test cell / reference cell combinations. The spectral responsivities of the test cells used for the data shown here were measured under light bias of ~ 1 sun. The effect of light bias intensity on spectral mismatch factor

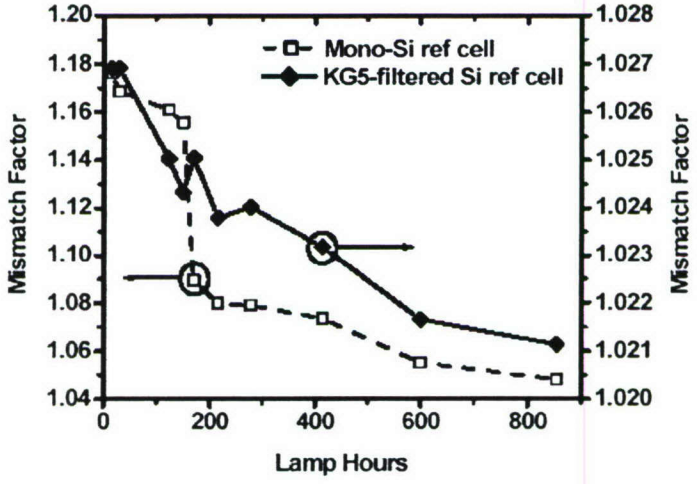

Figure 2. The change in spectral mismatch factor as a function of lamp age for a P3HT:PCBM(DCB) test cell. The mismatch is calculated for two reference cells: unfiltered and KG5 filtered Si diodes. The light source was a one sun Spectrolab X25 solar simulator.

(3) Conclusion

We have presented the methods for accurately rating the performance of organic solar cells. We discussed some of the important issues with respect to these devices, such as calculation and application of spectral mismatch factor for efficiency correction. Three different types of test cells and two reference cells were selected for calculating mismatch factors with respect to the AM 1.5 G reference spectrum. These typical spectral mismatch factors provide guidance in estimating spectral mismatch in different solar cell testing settings.

(4) References

1. C.J. Brabec, N.S. Sariciftci, and J.C. Hummelen, *Adv. Funct. Mater.* **11**, 15-26 (2001).
2. P. Peumans, A. Yakimov, and S.R. Forrest, *J. Appl. Phys.* **93**, 3693 (2003).
3. C.J. Brabec, V. Dyakonov, J. Parisi, and N.S. Sariciftci, in *Organic Photovotlaics: Concepts and Realization*, Springer (2003).
4. K.M. Coakley and M.D. McGehee, *Chem. Mater.* **16**, 4533-4542 (2004).
5. C.J. Brabec, *Solar Energy Mater. & Solar Cells* **83**, 273-292 (2004).
6. S.S. Sun and N.S. Sariciftci, in *Organic Photovoltaics: Mechanisms, Materials and Devices*, CRC (2005).
7. G. Yu, J. Gao, J.C. Hummelen, F. Wudl, and A.J. Heeger, *Science* **270**, 1789-1791 (1995).
8. N.S. Saraciftci, L. Smilowitz, A.J. Heeger, and F. Wudl, *Science* **258**, 1474-1476 (1992).
9. C.W. Tang, *Appl. Phys. Lett.* **48**,183 (1986).
10. L.J. Lutsen, P. Adriaensens, H. Becker, A.J. Van Breemen, D. Vanderzande, and J. Gelan, *Macromolecules* **32**, 6517 (1999).
11. S.E. Shaheen, C.J. Brabec, F. Padinger, T. Fromherz, J.C. Hummelen, and N.S. Sariciftci, *Appl. Phys. Lett.* **78**, 841 (2001).
12. M.M. Wienk, J.M. Kroon, W.J.H. Verhees, J. Knol, J.C. Hummelen, P.A. van Hal, and R.A.J. Janssen, *Angew. Chem. Int. Ed.* **42**, 3371 (2003).
13. T. Chen and R. D. Rieke, *J. Am. Chem. Soc.* **114**, 10087 (1992).
14. R.D. McCullough, R.D. Lowe, M. Jayaraman, and D.L. Anderson, *J. Org. Chem.* **58**, 904 (1993).
15. F. Padinger, R.S. Rittberger, and N.S. Sariciftci, *Adv. Funct. Mater.* **13**, 85 (2003).
16. D. Chirvase, J. Parisi, J.C. Hummelen, and V. Dyakonov, *Nanotechnology* **15**, 1317 (2004).
17. G. Li, V. Shrotriya, Y. Yao and Y. Yang, *J. Appl. Phys.* **98**, 043704 (2005).
18. G. Li, V. Shrotriya, J. Huang, Y. Yao, T. Moriarty, K. Emery, and Y. Yang, *Nat. Mater.* **4**, 864 (2005).
19. M. Reyes-Reyes, K. Kim, and D.L. Carroll, *Appl. Phys. Lett.* **87**, 083506 (2005).
20. W.L. Ma, C.Y. Yang, X. Gong, K. Lee, and A.J. Heeger, *Adv. Funct. Mater.* **15**, 1617 (2005).
21. N.S. Sariciftci, D. Braun, C. Zhang, V.I. Sradnov, A.J. Heeger, G. Stucky, and F. Wudl, *Appl. Phys. Lett.* **62**, 585 (1993).
22. S. Alem, R. de Bettignies, J.-M. Nunzi, and M. Cariou, *Appl. Phys. Lett.* **84**, 2178 (2004).
23. J.C. Hummelen, B.W. Knight, F. LePeq, F. Wudl, J. Yao, and C.L. Wilkins, *J. Org. Chem.* **60**, 532 (1995).
24. P. Peumans, S. Uchida, and S.R. Forrest, *Nature* **425**, 158-162 (2003).
25. J. Xue, S. Uchida, B.P. Rand, and S.R. Forrest, *Appl. Phys. Lett.* **85**, 5757 (2004).
26. F. Yang, M. Shtein, and S.R. Forrest, *Nature Materials* **4**, 37-41 (2005).
27. J. Drechsel, B. Männig, F. Kozlowski, D. Gebeyehu, A. Werner, M. Koch, K. Leo, and M. Pfeiffer, *Thin Solid Films* **451**, 515 (2004).

28. J. Drechsel, B. Männig, D. Gebeyehu, M. Pfeiffer, K. Leo, and H. Hoppe, *Org. Electron.* **5**, 175 (2004).
29. C.-W. Chu, Y. Shao, V. Shrotriya, and Y. Yang, *Appl. Phys. Lett.* **86**, 243506 (2005).
30. S. Yoo, B. Domercq, and B. Kippelen, *Appl. Phys. Lett.* **85**, 5427 (2004).
31. K. Emery and C. Osterwald, *Sol. Cells* **17**, 253 (1986).
32. K. Emery and C. Osterwald, *Current Topics in Photovoltaics*, Vol. 3, Chap. 4, Academic Press, London 1988.
33. K. Emery, in *Handbook of Photovoltaic Science and Engineering* (Ed: A. Luque and S. Hegedus), Chap. 16, John Wiley & Sons, Ltd., W. Sussex, 2003.
34. J. Rostalski and D. Meissner, *Sol. Energy Mater. Sol. Cells* **61**, 87 (2000).
35. J.M. Kroon, M.M. Wienk, W.J.H. Verhees, and J.C. Hummelen, *Thin Solid Films* **403-404**, 223 (2002).

Standard IEC 60904-1, Photovoltaic devices Part 1: Measurement of Photovoltaic Current-voltage Characteristics, International Electrotechnical Commission, Geneva, Switzerland.

Park 4 Effect of self-organization in polymer/fullerene bulk heterojunctions on solar cell performance

(1). Introduction

In the last decade, polymer photovoltaic (PV) cells have emerged as a promising source of non-conservative, renewable and truly clean energy.[1,2] PV devices based on a bulk-heterojunction (BHJ) of donor and acceptor components have shown the highest efficiencies reported so far. Among the most promising donor materials, that have found tremendous attention from the research community, is regioregular poly(3-hexylthiophene) or RR-P3HT. Highly efficient solar cells based on BHJ of P3HT with [6,6]-phenyl-C_{61}-butyric acid methyl ester (PCBM) have been demonstrated.[3-5] Recently, we reported very efficient plastic solar cells based on P3HT/PCBM where controlling the growth rate of the active layer resulted in a significant enhancement in device efficiency.[6] The slow growth of the active layer induced self-organization in the polymer chains, as a result of which significant improvement in the absorbance and the carrier mobility was observed. Here, we investigate in detail the mechanisms behind efficiency improvement in P3HT/PCBM devices. The effect of self-organization by slow growth on the active layer morphology is examined by atomic force microscope (AFM) technique. The transport properties of the materials are studied by fitting the current-voltage (J-V) characteristics measured under dark to the space-charge limited current (SCLC) model.[7,8] Single carrier (hole-only and electron-only) devices are fabricated to determine the charge carrier mobility in the active layer. Finally, the photocurrent behavior of PV devices under reverse bias is examined based on the Onsager's theory[9] of ion-pair dissociation in weak electrolytes. Reasonable fit to the experimental data is obtained for photocurrent as function of bias by varying the parameters involved in the model. The effect of growth rate on the dissociation efficiency of electron-hole (e-h) pair under short-circuit conditions are examined, and its effect on the device performance is discussed.

(2) Results and Discussion

Figure 1 shows the AFM phase images for P3HT/PCBM films that are grown at different rates. The images are obtained in tapping mode for a 1 μm × 1 μm surface area. The effect of growth rate on morphology of the active layer is clearly visible. The phase image of the fast grown film [Fig. 1 (a)] shows coarse chain-like features running across the surface. These features are assigned to the domains of pure P3HT crystallites each of which contains several polymer chains tightly packed. The region between these features consists of either P3HT/PCBM mixed domains or pure PCBM clusters. PCBM molecules suppress the formation of P3HT crystallites in the fast grown films and most of the film consists of mixed domains which are amorphous in nature. For the slow grown film, however, the crystalline domains of pure P3HT chains are denser and are distributed more uniformly throughout the film [Fig 1 (b)]. The separation distance between the features is also less, which suggests tighter packing of P3HT crystallites in the slow grown film. The separation distance between surface features in slow grown film (~ 28 nm) is smaller than that in fast grown film (~ 55 nm). The crystallite size estimated from AFM phase images matches the results

from XRD data on similar films[10,11] where mean crystallite size estimated from Scherrer's equation is 10-50 nm. The reduced crystallite size and inter-crystallite spacing are believed to be the result of higher ordering. P3HT chains get more time to self-organize into a more ordered structure during very slow growth. As a result, the regions of mixed P3HT/PCBM domains will reduce. Also, the AFM height images reported earlier for the fast and slow grown films show that the texture is rougher for the slow grown film.[6] The higher surface roughness of the slow grown film is also a signature of higher ordering due to self-organization in the polymer chains.[3,6]

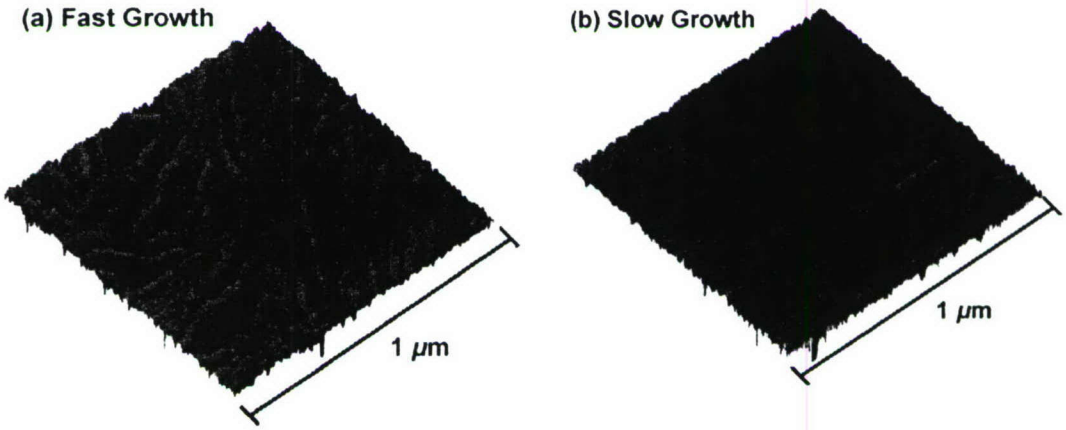

Figure 1. The effect of growth rate induced self-organization on the morphology of the active layer. AFM phase image of (a) fast grown and (b) slow grown polymer/fullerene blend film for a 1 μm × 1 μm surface area.

In polymer BHJ solar cells an important factor in determining external quantum efficiency is the carrier transport in the active layer. To make a realistic estimate of the carrier mobilities in the blend film and accurate comparison of electron and hole mobilities, it is important to perform the measurements on the same device configuration as the actual device. The electron and hole mobilities can be measured precisely by fitting the dark *J-V* curves for single carrier devices to SCLC model at low voltages, where the current is given by $J = 9\varepsilon_0\varepsilon_r\mu V^2/8L^3$ (Ref. 11), where $\varepsilon_0\varepsilon_r$ is the permittivity of the polymer, μ is the carrier mobility and L is the device thickness. Figure 2 shows the log *J*-log *V* curves for (a) hole-only and (b) electron-only devices where the active layer of P3HT/PCBM was obtained by slow and fast growth. The applied bias voltage is corrected for the built-in potential so that $V = V_{APPLIED} - V_{BI}$. Molybdenum oxide (MoO_3), with work function (Φ) = 5.3 eV as measured in our lab by ultra-violet photoelectron spectroscopy (UPS), is a good hole injection contact for P3HT/PCBM.[18] A large energy barrier between LUMO of PCBM and Φ of MoO_3 ($\Delta E \sim 1.6$ eV) suppresses electron injection from the top electrode rendering the device hole-only characteristics. Cesium carbonate (Cs_2CO_3) has been used as an efficient electron-injection layer for organic electroluminescent devices.[19] The work

function of Cs_2CO_3 was found to be ~ 2.9 eV by UPS measurements conducted in our lab. Therefore, it can replace polyethylenedioxythiophene: polystyrenesulfonate (PEDOT:PSS) as the anodic buffer layer to make electron-only devices. For the fast grown films the mobilities are $\mu_e \sim 6.5 \times 10^{-8}$ and $\mu_h \sim 1.9 \times 10^{-9}$ $m^2V^{-1}s^{-1}$. For slow grown film the electron mobility increases by four times to 2.6×10^{-7} $m^2V^{-1}s^{-1}$, but the hole mobility increases by about two orders of magnitude to 1.7×10^{-7} $m^2V^{-1}s^{-1}$. The ratio of electron to hole mobility is therefore ~ 1.5 times, which is similar to the observation from TOF measurements. A relatively small increase in μ_e (by 4 times) upon slow growth is understandable because the slow growth of the blend results primarily in an increased ordering in the polymer chains which will significantly effect the hole mobility, whereas it will have small effect on the electron mobility in PCBM. An increase of two orders in magnitude in μ_h upon slow growth further supports this argument.

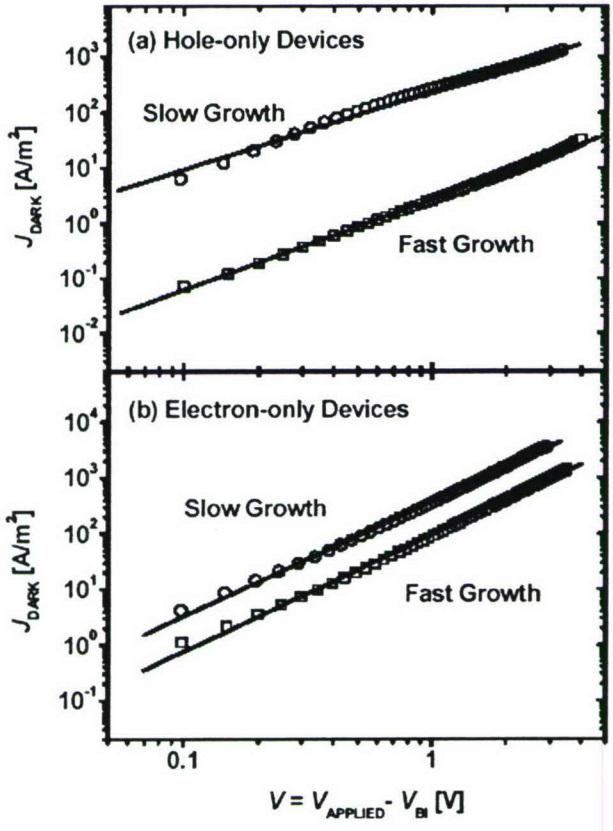

Figure 2. Measured *J-V* characteristics under dark for (a) hole-only and (b) electron-only PV devices consisting of P3HT/PCBM active layer grown at fast and slow rates. The solid lines represent the fit to the experimental data using SCLC model. The bias is corrected for built-in potential (V_{BI}), arising from difference in the work function of the contacts, so that $V = V_{APPLIED} - V_{BI}$. V_{BI} values are 0.1 V for both hole- and electron-only devices.

To study the effect of growth rate of the active layer on the photocurrent generation in the device, we measured the *J-V* characteristics in reverse bias under 100 mW/cm^2 simulated AM 1.5G conditions. The devices were biased in a sweep from + 0.8 V to -15.0 V. Figure 3 shows the photocurrent (J_{PH}) as a function of the effective applied bias, $V_{EFF} = V_0 - V$, where V is the applied bias. J_{PH} is the obtained by correcting the current under illumination for the dark current, i.e., $J_{PH} = J_{LIGHT} - J_{DARK}$, and V_0 is the bias where $J_{LIGHT} = J_{DARK}$. Also shown in the inset of Fig. 3 are the *J-V* characteristics under illumination for the fast and slow grown films. In the low effective field region ($V_{EFF} < 0.1$ V), the photocurrent increases linearly with voltage for both types of devices. Such behavior has been reported earlier for MDMO-PPV/PCBM system by Mihailetchi *et al.*[17,20] At large reverse bias ($V_{EFF} > 10$ V), J_{PH} saturates for both devices with saturation photocurrent (J_{SAT}) of ~ 125 A/m^2 for the fast and ~ 155 A/m^2 for the slow grown film. The maximum generation rate (G_{max}) (given as $J_{SAT} = eG_{max}L$) is 3.5×10^{27} m^{-3}s^{-1} and 4.4×10^{27} m^{-3}s^{-1} for the fast and slow grown films (thickness $L = 220$ nm). Upon changing the growth rate of the film from fast to slow, the *e-h* pair generation in the film increases by about 26 %. This increase is attributed to the increased absorption in the active layer when the film is grown slowly.[6] However, what is more interesting here is the difference in the behavior of photocurrent in the intermediate voltage regime ($0.1 < V_{EFF} < 10$ V) for fast and slow grown films.

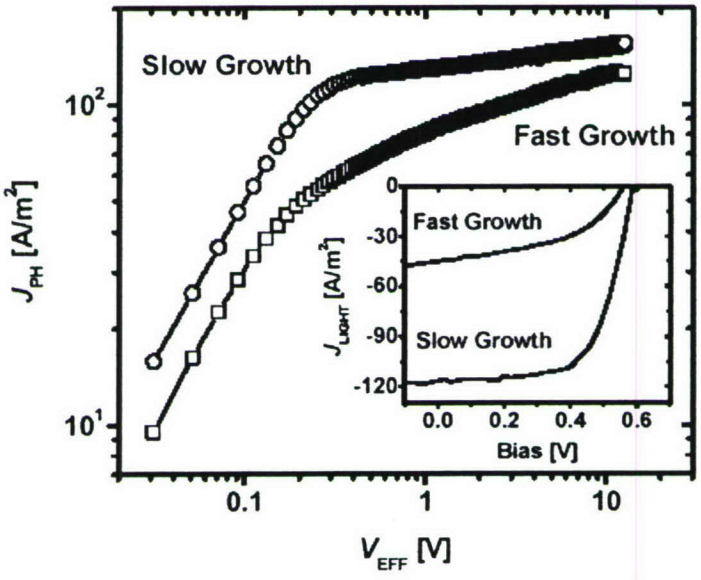

Figure 3. Measured photocurrent as a function of effective applied bias for PV devices with fast and slow grown active layer. The *J-V* characteristics under illumination (130 mW/cm^2, simulated AM 1.5G) for two PV devices with different active layer growth rates are shown in the inset.

To compare the photocurrent behavior, we have plotted the normalized photocurrent (J_{PH}/J_{SAT}) for the fast and slow grown films in Fig. 4 (a) and (b). The short-circuit operation point ($V_{EFF} = V_0$) for both types of devices is marked by a

dashed line parallel to the y-axis in the figures. At any given electric field and temperature, only a certain fraction of photogenerated *e-h* pairs will dissociate into free carriers with dissociation probability $P(E,T)$. This gives the generation rate at any given electric field and temperature as $G(E,T) = G_{max} P(E,T)$, and the photocurrent as $J_{PH} = eG_{max} P(E,T)L$.[20] Onsager's theory[9] of ion-pair dissociation in weak electrolytes, modified by Braun[21], has been used in the past to describe the J_{PH}-V behavior in MDMO-PPV/PCBM solar cells.[20] First we examine the J_{PH}-V behavior for the fast grown film. From the Onsager's model, an exact fit to the experimental data can be obtained in the complete bias range (solid curve). From the J_{PH}/J_{SAT} data, the *e-h* pair dissociation efficiency at any bias can be calculated. At the short-circuit condition (V = 0, or V_{EFF} = V_0), only 57 % of the total photo-generated *e-h* pairs dissociate into free carriers, which further reduces to 41 % at the maximum power output point (V = 0.4 V). This suggests that more than half of the *e-h* pairs that are generated after photo-induced charge transfer are lost due to recombination in the active layer, before they can be separated into free carriers. On the other hand, the photocurrent behavior of the slow grown film shows some very interesting features. A good fit to the experimental data can be obtained from Onsager's model within the bias range of 0.1 V < V_{EFF} < 10 V, but a current slightly higher than the experimental data is calculated in the low bias regime (V_{EFF} < 0.1 V). At the short-circuit condition, the e-h pair dissociation efficiency is more than 80 %, which is probably the highest value observed in a polymer BHJ device so far. At the maximum power output bias, the efficiency is still around 70 %. Such high dissociation efficiency numbers clearly demonstrate the effect of self-organization induced ordering in the blend films. It is also interesting to note the steeper field dependence of generation rate in the low to mid-range fields for the slow grown film. The J_{PH}/J_{SAT} curve shows saturation behavior at very low bias and does not increase much after this point. This behavior is very similar to the observation made by Goliber and Perlstein[22] where they used a delta distribution function, instead of a Gaussian, for the charge-transfer (CT) radii. As discussed before, the slow grown films show a higher degree of ordering because of self-organization in the polymer chains. As a result, the donor-acceptor separations (or the separation between the polymer and PCBM phases) throughout the film is expected to be much more uniform as compared to the fast grown film where the distribution is supposed to be more dispersed. The observed steep variation of J_{PH} in a small bias range for the slow grown film therefore supports the argument of more ordering in the blend system. It is worth mentioning that the mean CT radii are the same (~ 1.7 nm) for both types of films, but a delta distribution of donor-acceptor separations is expected in case of slow grown films instead of Gaussian distribution for fast grown films.

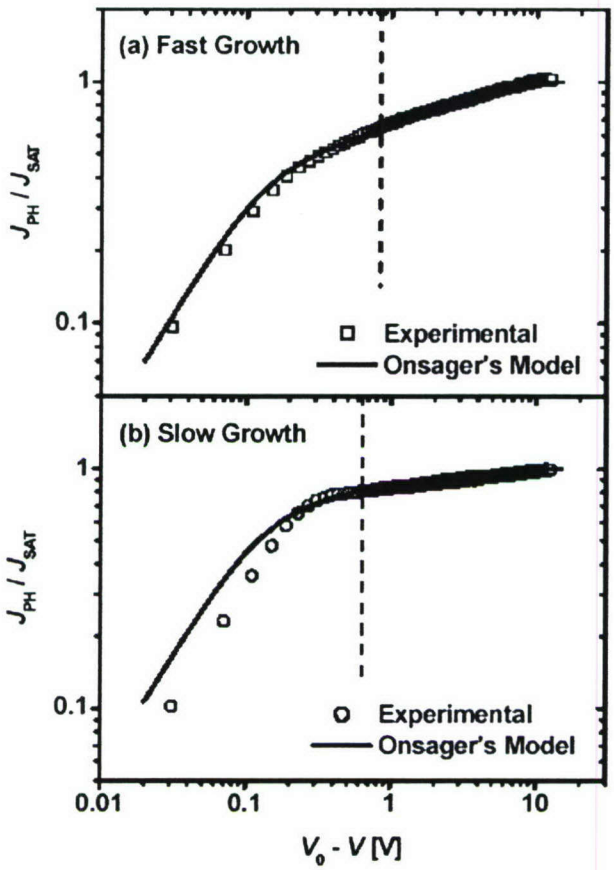

Figure 4. Measured (open symbols) and calculated (solid curves) normalized photocurrent as a function of effective applied bias for (a) fast and (b) slow grown films. The solid curves represent the J_{PH}/J_{SAT} values calculated from the Onsager's model.

(3) Conclusion

Based on the mobility and photocurrent measurements discussed above, we conclude that the effect of growth rate on the performance is understood to be threefold - higher exciton generation, higher dissociation efficiency of *e-h* pair (up to 80 %), and increase in hole mobility by roughly two orders of magnitude which coupled with a four-fold increase in the electron mobility results in a highly balanced charge transport. The ordering induced in the active layer because of self-organization opens an important direction in the efforts to increase the performance of polymer BHJ solar cells. Donor conjugated polymers similar to P3HT that can form self-organized crystalline structures should be the focus of attention to increase the efficiency levels beyond the current values.

List of Publications

1. Ricky J. Tseng, Christina O. Baker, Brian Shedd, Jiaxing Huang, Richard B. Kaner, Jianyong Ouyang, and Yang Yang, "Charge transfer effect in the polyaniline-gold nanoparticle memory system", Appl. Phys. Lett. 90, 053101 (**2007**).
2. R. J. Tseng, J. Ouyang, C. W. Chu, J. Huang, and Y. Yang, "Nanoparticle-induced negative differential resistance and memory effect in polymer bistable light-emtting device", Appl. Phys. Lett. 88, 123506 (**2006**)
3. Ricky J. Tseng, Chunglin Tsai, Liping Ma, Jianyong Ouyang, Cengiz S. Ozkan, and Yang Yang, "Digital memory device based on tobacco mosaic virus conjugated with nanoparticles", Nature Nanotech. 1, 72 (**2006**)
4. Ankita Prakash, Jianyong Ouyang, Jen-Lien Lin, and Yang Yang, "Polymer memory device based on conjugated polymer and gold nanoparticles", J. Appl. Phys. 100, 054309 (**2006**)
5. Yang Yang, Jianyong Ouyang, Liping Ma, Ricky Jia-Hung Tseng, and Chih-Wei Chu, "Electrical Switching and Bistability in Organic/Polymeric Thin Films and Memory Devices", Adv. Func. Mater. 16, 1001–1014 (**2006**)
6. Vishal Shrotriya, Gang Li, Yan Yao, Tom Moriarty, Keith Emery, and Yang Yang. Accurate Measurement and Characterization of Organic Solar Cells. ADVANCED FUNCTIONAL MATERIALS, 16, 2016–2023, (2006).
7. Jinsong Huang, Wei-Jen Hou, Juo-Hao Li, Gang Li and Yang Yang, Improving the power efficiency of white light-emitting-diode by doping electron transport material, Appl. Phys. Lett. 89, 133509 (2006).
8. Juo-Hao Li, Jinsong Huang, and Yang Yang, Improved hole-injection contact for top-emitting polymeric diodes, Appl. Phys. Lett. 90, 173505 (2007).
9. Gang Li, Vishal Shrotriya, Jinsong Huang, Yan Yao, Tom Moriarty and Keith Emery and Yang Yang, "High efficiency solution processable polymer photovoltaic cells by self-organization of polymer blends", Nature Materials, 4, 865, (**2005**)*
10. Yan Shao and Yang Yang, "Efficient organic hetero-junction photovoltaic cells based on triplet materials", Adv. Mat., 17, 2841-44, (**2005**)
11. Seungmoon Pyo, Liping Ma, Jun He, Qianfei Xu, Yang Yang, Yongli Gao "Experimental study on thickness-related electrical characteristics in organic/metal-nanocluster/organic systems", J. Appl. Phys. 98, 054303, (**2005**).*
12. Liping Ma and Yang Yang, "Solid-state supercapacitors for electronic device applications", Applied Physics Letters, 87, 123503 - 05. (**2005**)*
13. Jinsong Huang, Gang Li, and Yang Yang, "Influence of composition and heat-treatment on the carriers transport properties of poly(3-hexylthiophene) [6,6]-phenyl C61-butyric acid methyl ester", Appl. Phys. Lett. 87, 112105, (**2005**)*
14. Gang Li and Yang Yang, "Investigation of annealing effects and thickness dependence of solar cells based on poly(3-hexylthiophene)", J. Appl. Phys., 98,

043704-08, (**2005**)*
15. Jianyong Ouyang, CHIH-WEI CHU, RICKY JIA-HUNG TSENG, ANKITA PRAKASH, and Yang Yang, "Organic Memory Device Fabricated Through a Solution Processing", IEEE Proceeding, 93, pp 1287- 1296, (**2005**)*
16. Elbert Wu, Sheng-Han Li, Chieh-Wei Chen, Gang Li, Zheng Xu,, and Yang Yang,, "Controlling Optical Properties of Electrodes With Stacked Metallic Thin Films for Polymeric Light-Emitting Diodes and Displays", IEEE J. Display Technology., 1,p.p. 105-111, (**2005**)*
17. V. Shrotriya, J. Ouyang, R. J. Tseng, G. Li, and Y. Yang, "Absorption spectra modification in poly(3-hexylthiophene):methanofullerene blend thin films ", Chem. Phys. Lett. **411**, 138 (**2005**)*
18. Yan Shao and Yang Yang, "Organic solid solution: formation and application in organic light emitting diodes", Advanced Functional Materials, 15, 1781-1786, (**2005**)*
19. Chihwei Chu and Yang Yang, "An effective connecting structure for tandem OLEDs", Appl. Phys. Lett., 86, 253503, (**2005**)*
20. Chih-Wei Chu, Yan Shao, Vishal Shrotriya, and Yang Yang, "Efficient photovoltaic energy conversion in tetracene-C60 based heterojunctions", Appl. Phys. Lett. 86, 243506, (**2005**)*
21. Qianfei Xu, Jinsong Huang, and Yang Yang, "Highly efficient polymer LED", J. Soc. Inf. Display **13**, 411 (**2005**)*
22. Jiahung Tseng, Jianyong Ouyang, Jiaxing Huang, Richard Kaner, and Yang Yang, "Polyaniline nano-fiber nonvolatile digital memory" , Nano Letters, , **5**, 1077 (**2005**)
23. Chihwei Chu, Jianyong Ouyang, Jiahung Tzeng, Yang Yang, "Organic Donor-Acceptor System Exhibiting Electrical Bistability for Use in Memory Devices", Advanced Materials, **17**, 11, 1440 (**2005**).*
24. Shenghan Li and Yang Yang, "Stacked metal cathode for high contrast ratio polymeric-light emitting diodes", Appl. Phys. Lett., **86**, 143514 , (**2005**)*
25. Jianyong Ouyang, Chih-Wei Chu, Douglas Sieves, and Yang Yang, "Electric-field induced charge transfer between gold nanoparticle and capping 2-naphthalenethiol and organic memory cells", Appl. Phys. Lett., **86**, 123507 (**2005**).
26. Jun He, Liping Ma, Jianhua Wu and Yang Yang, "Three-Terminal Organic Memory Devices", J. Appl. Phys. **97**, 064507 (**2005**).*
27. Meng Lu, Baohan Xie, Jeonghee Kang, and Zhonghua Peng, Fang-Chung Chen, and Yang Yang, Synthesis of Main-Chain Polyoxometalate-Containing Hybrid Polymers, Chemistry of Materials, **17**, 402 (**2005**).
28. Kevin Cheng, Ming-Huan Yang, Wanda W. W. Chiu, Chieh-Yi Huang, Jane Chang, Tai-Fa Ying, Yang Yang, "Ink-jet Printing, Self-assembled Polyelectrolytes, and Electroless Plating: Low Cost Fabrication of Circuits on Flexible Substrate at Room Temperature", Macromolecular Rapid Communication, **26**, 247 (**2005**)
29. Vishal Shariarty and Yang Yang, "Capacitance-voltage analysis of defect density in polymer LEDs", J. Appl. Phys. **97**, 054504 (**2005**).
30. Yan Shao and Yang Yang, "White organic light-emitting diodes prepared by a

fused organic solid solution method", Appl. Phys. Lett. **86**, 073510 (**2005**)
31. Jianyong Ouyang, Chiwei Chu, Fang-Chung Chen, and Yang Yang, "High-conductivity poly(3,4-ethylenedioxythiophene): polystyrenesulfonate film and its application in polymer optoelectronic devices", Advanced Functional Materials, **15**, 203. (**2005**).
32. Jianyong Ouyang, Chih-Wei Chu, Charles R. Szmanda, Liping Ma, and Yang Yang, Programmable polymer thin film and non-volatile memory device, **Nature Materials**, November, 28, 1-5(2004).

List of Patents filed

(1) Y. Yang, J. Ouyang, and C. Szmanda, "Memory devices based on electric field programmable films", pending.
(2) Y. Yang and J. Ouyang, "Write-once-read-many plastic memory", pending.
(3) Yang Yang and Liping Ma,, Vertical organic field effect transistor, WO2005024907 - 2005-03-17 (licensed by ORFID Corp.)

(4) Yang Yang and Liping Ma, Novel capacitors and devices incorporating the capacitors UCLA 2005-305-1, 60/709.931, filing date: August 21, 2006.

(5) Yang Yang, Sheng-Han Li, Liping Ma, Ambipolar vertical organic field-effect transistors, UCLA 2005, U.S. Provisional Application No. 60/728,742, filed October 21, 2006.

(6) Yang Yang, Gang Li, "High Efficiency Polymer Photovoltaic Cells Prepared by Self-Organization of Polymer Composite", U.S. Provisional Application No. 60/669,332 UCLA Reference: 2005-524-1

(7) Yang Yang and Gang Li, "Photon-Conversion Materials (PCMs) in Polymer Solar Cells – Enhance Efficiency and Prevent Degradation",U.S. Provisional Application No. 60/774,188, UCLA Reference: 2006-453-1.

(8) Yang Yang, Jinsong Huang, A General Method for Achieving High Efficiency in Polymer Light-Emitting Diodes. (2005)

B. Program Statistics

[1]. Number of PI and Co-PI involved in the research project: 2

[2]. Number of Post Doc Supported in the last 12 months under AFOSR: 2

[3]. Number of graduate students supported in the last 12 months by AFOSR: 4

[4]. Other researchers supported in the last 12 months by AFOSR: 2

[5]. Number of publications by PI's in the last 12 months period in refereed journals: 25

[6]. Number of publications in the last 12 months (in refereed journals only) that acknowledge AFOSR supports:14

[7]. Awards and Honors received by the PI (life-time received):

1. Outstanding Overseas Chinese Scientist, Natural Science Foundation-China, (2004)
2. Outstanding Alumni Award, U-Mass Lowell, (1999)
3. NSF Career Award, (1998);
4. 3M Young Investigator Award, (1998);